Materials Today Bio 18 (2023) 100527

Contents lists available at ScienceDirect

Materials Today Bio

journal homepage: www.journals.elsevier.com/materials-today-bio

Mechanical stimulation on a microfluidic device to highly enhance small extracellular vesicle secretion of mesenchymal stem cells

Rui Hao [a,1], Shi Hu [b,1], Huitao Zhang [b], Xi Chen [b], Zitong Yu [b], Jingyi Ren [b], Hang Guo [a,**], Hui Yang [b,*]

[a] Pen-Tung Sah Institute of Micro-Nano Science and Technology, Xiamen University, Xiamen, 361005, China
[b] Laboratory of Biomedical Microsystems and Nano Devices, Center for Bionic Sensing and Intelligence, Institute of Biomedical and Health Engineering, Shenzhen Institute of Advanced Technology, Chinese Academy of Sciences, Shenzhen, 518055, China

ARTICLE INFO

Keywords:
Microfluidics
Small extracellular vesicles
Mechanical squeezing
Secretion amount
Mesenchymal stem cells

ABSTRACT

Small extracellular vesicles (sEVs) are recognized as promising detection biomarkers and attractive delivery vehicles, showing great potential in diagnosis and treatment of diseases. However, the applications of sEVs are usually restricted by their poor secretion amount from donor cells under routine cell culture conditions, which is especially true for mesenchymal stem cells (MSCs) due to their limited expansion and early senescence. Here, a microfluidic device is proposed for boosting sEV secretion from MSCs derived from human fetal bone marrow (BM-MSCs). As the cells rapidly pass through a microfluidic channel with a series of narrow squeezing ridges, mechanical stimulation permeabilizes the cell membrane, thus promoting them to secrete more sEVs into extracellular space. In this study, the microfluidic device demonstrates that mechanical-squeezing effect could increase the secretion amount of sEVs from the BM-MSCs by approximately 4-fold, while maintaining cellular growth state of the stem cells. Further, the secreted sEVs are efficiently taken up by immortalized human corneal epithelial cells and accelerate corneal epithelial wound healing *in vitro*, indicating that this technique wound not affect the functionality of sEVs and demonstrating the application potentials of this technique.

1. Introduction

Small extracellular vesicles (sEVs), a subtype of EVs referred to the size less than 200 nm, are lipid bilayer-enclosed nanovesicles naturally secreted by almost all cell types into extracellular environment [1,2]. Although the sEVs were initially regarded as only a waste cleaner for cellular metabolism, they are now recognized as a critical signal mediator responsible for information transmission and substance delivery between cells [3–5]. As intercellular cargo vehicles, sEVs not only play a significant role in physiological processes involving inflammation suppression, regulation of cell proliferation, angiogenesis, tissue repair, etc., but also deeply involve in pathogenesis of cancer, neurodegenerative diseases, cardiovascular diseases, infection diseases, etc. [6–9] Therefore, sEVs can be used as promising biomarkers to study the mechanism of various physiological and pathological activities [10], and can serve as natural carriers to deliver exogenous cargos, including chemical drugs, nucleic acids, proteins, and nanomaterials [11–14]. Despite a great potential of sEVs in biomedical researches, their practical applications are greatly hindered by a critical technical challenge lying in the trivial secretion amount of sEVs from donor cells [3,15]. This obstacle is especially true for mesenchymal stem cells (MSCs) because of their limited cell expansion capability [16]. After a few passages, the non-immortalized MSCs are gradually senescent, which may alter functionality of the secreted sEVs [17].

In order to enhance the secretion amount of sEVs, several attempts have been made, such as cytokine regulation, ethanol stimulation, oxidative stress, etc. [18–21] However, these methods require additional biological or chemical agents in the cell culture system, altering the physiological status of the donor cells and thereby affecting the functionality of secreted sEVs [7,15]. In addition, physical stimulation serves as a promising alternative and avoid the additives. Several groups have tried to increase the secretion amount of sEVs based on physical stimulation techniques, such as laser irradiation, ultrasound stimulation, electricity effect, mechanical turbulence, etc. [9,22–25] However, these

* Corresponding author.
** Corresponding author.
E-mail addresses: hangguo@xmu.edu.cn (H. Guo), hui.yang@siat.ac.cn (H. Yang).
[1] These authors contributed equally: Rui Hao, Shi Hu.

https://doi.org/10.1016/j.mtbio.2022.100527
Received 20 August 2022; Received in revised form 21 December 2022; Accepted 22 December 2022
Available online 24 December 2022

techniques usually require high-end, expensive, and bulky setups, leading to low sample throughput, inconsistent cell stimulation, insufficient nutrition supply, and damaged cell viability [26,27].

On the other hand, micro-/nano-fluidic technologies offer the ability to localize physical fields to cellular or subcellular scales, and thus achieving more precise and homogeneous physical stimulation [28]. For example, cellular nanoporation platform, which permeabilizes cell membrane by nanochannel electroporation stimulation, was verified to significantly increase the secretion amount of sEVs from different cell types [29,30]. Alternatively, microfluidic cell squeezing can also permeabilize cell membranes, improving sample throughput while avoiding low cell viability, Joule heating, and metal contamination [28,31], showing great application prospects in boosting sEV secretion [32,33]. These techniques indicate that cells are well equipped to deal with membrane disruption, this has been verified by latest study of membrane repair pathways. Therefore, microfluidic-based mechanical squeezing technique also holds great potential in secretion improvement of sEVs by permeabilizing the cell membrane. Here we investigate a microfluidic device to efficiently improve sEV secretion from human fetal bone marrow-derived MSCs, and study the sEVs on corneal epithelial wound healing.

2. Materials and methods

2.1. Cell culture

MSCs derived from human fetal bone marrow (BM-MSCs) were purchased from Cyagen Biosciences. The cells were grown in the OriCell medium consisting of 89% (*v/v*) OriCell basal medium, 10% (*v/v*) OriCell fetal bovine serum (FBS), and 1% (*v/v*) OriCell penicillin-streptomycin (PS). According to the manufacturer's instructions, the BM-MSCs at passage 7 or earlier were used in all of the experiments. In addition, immortalized human corneal epithelial cells (iHCECs) were purchased from RIKEN BioResource Research Center and grown in DMEM/F-12 (Gibco) supplemented with 6% (*v/v*) FBS (Gibco), 1% (*v/v*) PS (Gibco), and 10 ng/mL recombinant human epidermal growth factor (PeproTech). Both cells were cultured at 37 °C in a humidified incubator (Heracell 150i, ThermoFisher) with an atmosphere of 5% CO_2/95% air (*v/v*).

2.2. Fabrication and operation of the SEED

The polydimethylsiloxane (PDMS)-based microfluidic devices were made by soft lithography replica molding method [32,34]. Briefly, a reusable SU-8 photoresist (MicroChem) master was fabricated on a silicon wafer (RDMICRO) by a two-step photolithography process on a mask aligner (EV610, EV Group). Then, a 10:1 (*w/w*) PDMS mixture solution (Dow Corning) of prepolymer and curing agent was poured onto the SU-8 mold and degassed. After curing at 80 °C overnight, the PDMS replica was peeled off and punched to create inlet/outlet holes. Next, the PDMS layer with a microfluidic channel was bonded to a clean glass substrate via a plasma cleaner (PDC-MG, WEIKE). To prevent microbial contamination, the device was sequentially sterilized with ultraviolet light and 75% (*v/v*) ethanol, followed by a washing step with sterile deionized water (see Supplementary information section S2 for more details).

Further, BM-MSCs were collected from T25 cell culture flasks (Corning) and resuspended in OriCell medium supplemented with 10% (*v/v*) EV-depleted FBS (VivaCell). Size distribution of the cells was measured by an automated cell counter (Countess 3, Invitrogen), the average relaxed cell diameter was about 16 μm, whilst 73% cells were of 14–18 μm in diameter (see Supplementary information section S3 for more details). Then, the cell suspension with a concentration of 2×10^6 cells/mL were injected into SEED and driven through the microfluidic channel at different flow rates. After collected from the device outlet, these BM-MSCs were recovered at room temperature for 5–10 min, followed by a washing step with fresh EV-free medium [31,35]. Next, 5×10^5 of device-treated cells were seeded in a T25 cell culture flask and re-cultured in a humidified incubator for 48 h, which was determined by a dynamic quantitative analysis (see Supplementary information section S5 for more details). For the control group, BM-MSCs not treated by SEED but incubated in the medium were seeded in a flask at the same density and cultured under the same condition to set the base level of sEV secretion. In addition, to observe the squeezing-induced permeabilization of cell membrane, SEED-treated cell samples were imaged by scanning electron microscopy (SEM, Gemini Sigma 300, Zeiss).

2.3. Numerical simulations

Flow field distribution within the microfluidic channel was simulated by COMSOL Multiphysics software (COMSOL 5.3a, COMSOL) based on finite element analysis (FEA). According to device layout, a two-dimensional model was established along the middle cross-section of the microfluidic channel with 10 fishbone-shaped squeezing ridges. The computational study of flow field was modeled using steady Navier-Stokes equation combined with continuity equation for laminar flow of incompressible fluid. Input flow rate at the device inlet in the experiments can be defined from the calculated flow velocity profile inside the microfluidic channel (see Supplementary information section S5 for more details).

2.4. Isolation and characterization of sEVs

Cell morphology of SEED-treated and untreated BM-MSCs were observed via an inverted fluorescence microscopy (Axio Observer 7, Zeiss) after culturing. Then, 5 mL of cell culture supernatant was harvested from a T25 cell culture flask, followed by a differential ultracentrifugation to isolate sEVs [3,36]. Briefly, cell culture supernatant was centrifuged at 300×*g* for 10 min, 2000×*g* for 20 min, 4 °C, and 10,000×*g* for 30 min, 4 °C (FC5816R, OHAUS), subsequently. Then, the resulting supernatant was ultracentrifuged twice at 100,000×*g* for 70 min, 4 °C (Optima XE-100, Beckman Coulter) to purify sEVs (see Supplementary information section S6 for more details). Next, the pelleted sEVs were resuspended in the filtered PBS (Gibco) or medium for subsequent experiments.

Size and concentration of sEV samples were determined by Flow NanoAnalyzer (N30E, NanoFCM) following manufacturer's instructions. Measurement results were analyzed by NanoFCM software (Profession V1.0, NanoFCM) to calculate sEV concentration, secretion amount and size distribution. Moreover, average number of sEVs secreted from each BM-MSC was calculated by dividing the total number of sEVs by the number of BM-MSCs measured after re-culturing for 48 h (see Supplementary information section S9 for more details). In addition, morphology and protein markers (i.e., CD81, CD9, TSG 101, and Calnexin) of sEVs were characterized by transmission electron microscopy (Tecnai G2 spirit TEM, FEI) and western blot analysis, respectively, where GAPDH was used as internal reference. The protein amount of sEVs was also quantified by an BCA protein assay kit (Beyotime). Further, expression levels of microRNA (miRNA) content in sEV samples were evaluated by real-time quantitative polymerase chain reaction (RT-qPCR), and eight miRNAs involving in corneal epithelial wound healing were analyzed, including hsa-miR-21-5p, hsa-miR-138-5p, hsa-miR-106a-5p, hsa-miR-99b-3p, hsa-miR-19b-3p, hsa-miR-28-5p, hsa-miR-24-3p, and hsa-miR-151a-3p.

2.5. Evaluation of cell viability and stemness

Cell viability of BM-MSCs was assessed using a trypan blue exclusion test after the collection of cell culture supernatant [15,37]. In brief, cells in culture flasks were detached with 0.25% trypsin-EDTA (Gibco), resuspended with PBS, and stained using 0.4% (*w/v*) trypan blue solution

(Sigma-Aldrich). Then, the number of live and dead BM-MSCs were quantitatively measured by an automated cell counter. Cell viability was then calculated by dividing the number of live cells by total.

Further, analysis on BM-MSCs' stemness was performed using a human MSC surface marker detection kit (Cyagen). Referring to the previous works [38,39], six typical surface markers were selected, among which CD44, CD73, and CD105 were used as BM-MSC-positive markers, CD11b, CD34, and CD45 were used as negative markers (see Supplementary information section S8 for more details). Cells expressing MSC surface-specific markers were then measured by flow cytometer (NovoCyte 2060R, ACEA Biosciences) and the results were analyzed by NovoExpress software (Agilent).

2.6. Cellular uptake of sEVs

iHCECs were seeded into 8-well chambered cover-glass plates (ThermoFisher) at a density of 1.5×10^4 cells per well and cultured in a humidified incubator for overnight. The sEV samples collected from untreated and SEED-treated BM-MSCs were labeled with 3 μM lipophilic fluorescent dye PKH26 (excitation peak: 551 nm, emission peak: 567 nm, Sigma-Aldrich) according to the manufacturer's protocol. After incubating at room temperature for 10 min, sEVs were ultracentrifuged at 100,000×*g* for 90 min to remove excess dye molecules, followed by resuspending in DMEM/F-12 supplemented with 6% (*v/v*) EV-depleted FBS. Then, 300 μL of PKH-26 labeled sEV samples were added into each well and co-incubated with iHCECs at 37 °C for 14 h in humidified incubator. Next, iHCECs were washed with PBS, fixed with 4% (*w/v*) paraformaldehyde (PFA) solution (Beyotime), and stained with DAPI (excitation peak: 364 nm, emission peak: 454 nm, Beyotime). After washing with PBS, iHCECs were observed by an Axio Observer 7 inverted fluorescence microscopy (see Supplementary information section S10 for more details). The images were analyzed using Image-Pro Plus 6.0 software (Media Cybernetics) to quantify the fluorescent intensity and observe the distribution of PKH26-labeled sEVs.

2.7. In vitro scratch closure assay

A scratch closure assay was performed to investigate the effect of sEVs derived from SEED-treated BM-MSCs on iHCEC migration. Briefly, iHCECs were seeded into 24-well culture plates (SPL Life Science) at a density of 1.8×10^5 cells per well. After adhering for 6 h, iHCECs were serum-starved and grown overnight to 90% confluence. Then, the cell monolayers were scrathed along the central line of each well using a scratcher (SPL Life Science). Next, the scratched cell monolayers were cultured in the sEV sample derived from SEED-treated BM-MSCs, sEV sample isolated from untreated BM-MSCs, 4-fold diluted sample of the SEED group, and serum-free DMEM/F12, respectively. After 0–30 h of incubation, wound closure and cell migration were imaged serially using the Axio Observer 7 inverted fluorescence microscopy (see Supplementary information section S11 for more details). Images were analyzed using Image-Pro Plus 6.0 software to quantify the wound area and the migration area.

Further, the effects of sEVs secreted by the SEED-treated BM-MSCs on gene expression of the iHCEC cytokines were further investigated by RT-qPCR. After incubation with four different samples overnight, the scratched cell monolayers were washed twice with PBS, followed by extraction of total RNA with QIAzol Lysis Reagent (QIAGEN) according to manufacturer's protocol. RNA concentration was measured using a spectrophotometer (DS-11 FX, DeNovix). Then, RT-qPCR analysis on gene expression of cytokines related to corneal epithelial wound healing (i.e., interleukin-6 (IL-6), transforming growth factor-beta 1 (TGF-β1), and zona occludens-1 (ZO-1) was performed on a thermal cycler (qTOWER^3 G, Analytik Jena).

2.8. In vitro cell proliferation assay

5-ethynyl-2′-deoxyuridine (EdU) assay was performed to investigate sEVs secreted from SEED-treated BM-MSCs on proliferation of iHCECs [40,41]. The iHCECs were seeded into 8-well chambered cover-glass plates at a density of 1.2×10^4 cells per well. After adhering for 6 h, cells were serum-starved and grown overnight in serum-free DMEM/F-12. Then, iHCECs were incubated with four different samples, respectively. After 18 h of incubation, they were labeled with EdU solution (Beyotime), fixed with 4% (*w/v*) PFA solution, permeated by 0.3% (*v/v*) Triton X-100 solution (Sigma-Aldrich), labeled with click reaction buffer with Azide Alexa Fluor 647 (excitation peak: 650 nm, emission peak: 670 nm, Beyotime), and stained by Hoechst 33,342 (excitation peak: 346 nm, emission peak: 460 nm, Beyotime), subsequently. Next, proliferation of iHCECs were observed by Axio Observer 7 inverted fluorescence microscopy (see Supplementary information section S12 for more details). Fluorescence images were counted by Image-Pro Plus 6.0 software to analyze the rates of EdU positive cells (the number of EdU-labeled cells divided by the total number of cells labeled by Hoechst 33,342).

Further, iHCEC proliferation was also measured using a CCK-8 assay following previous protocols [11,42]. In brief, iHCECs adhered in 96-well plates (Corning) with a density of 4×10^3 cells per well were treated with four different samples, respectively, for 18 h. Then, 10 μL of CCK-8 solution was added into each well and incubated with iHCECs at 37 °C for 4 h. The optimal density (OD) value at 450 nm was measured using a microplate reader (Synergy H1, BioTek).

2.9. Statistical analysis

Statistics data are presented as mean ± standard deviation (SD) of three independent replicates. Statistical analysis was performed with one-way ANOVA with Tukey *post hoc* test (Originpro 2018 software, OriginLab) for multiple comparison. The statistical significance, high statistical significance, and no statistical significance are defined as $P < 0.05$ (*), $P < 0.01$ (**), and NS, respectively.

3. Results

3.1. Design and working principle

We developed a microfluidic device named "Small Extracellular vEsicles Developer (SEED)" to promote sEV secretion from cells by the stimulation of mechanical squeezing. Layout of SEED is illustrated in Fig. 1A (more details described in the Supplementary information section S1). The device consisted of four identical microfluidic channels with height of 25 μm for processing multiple samples in rapid succession. Each microfluidic channel integrated 10 fishbone-shaped squeezing ridges with height of 17 μm that were fabricated on a PDMS layer by soft lithography (more details presented in Materials and methods). The ridge gap between the bottom of the squeezing ridge and the top of the glass slide was used as the cell squeezing unit, where its size was set to 8 μm (optimal operating parameter). As cells rapidly pass through the microfluidic channel with ridge gap height smaller than cell size (Fig. 1B), mechanical squeezing can effectively permeabilize the cell membrane (Fig. 1C), thus stimulating cells to secrete more sEVs into extracellular space (Fig. 1D) [32,43,44]. Ten squeezing ridges were used to repeatedly exert mechanical compression to effectively permeabilize cell membrane while avoid damaging cell viability (Fig. S4). A fishbone-shaped layout was designed to focus cells to the center of the microfluidic channel and to self-clear cell aggregates in the meanwhile. SEED was operated at a sample throughput of 1×10^5 cells/min for 30 min without obvious clogging inside the microfluidic channel.

Mesenchymal stem cells derived from human fetal bone marrow (BM-MSCs) were chosen to be stimulated by SEED due to their tissue regeneration potential [3,8,17]. BM-MSCs suspended in medium (Fig. 1E) were introduced into the microfluidic channel through device inlet. There are multiple squeezing ridges inside the channel with the ridge gap smaller than cell size. As cells rapidly passed through the microfluidic channel, they were repeatedly mechanically deformed by periodic squeezing ridges, resulting in transient membrane disruption and cell permeabilization (Fig. 1F). Thereafter, the treated BM-MSCs were collected from device outlet and re-cultured in cell culture flasks (Fig. 1G).

3.2. Performance characterization

Since the permeability of cell membrane is regulated by the strength of mechanical squeezing, the relation between sEV secretion and squeezing parameters was studied. Gap height and flow velocity are two important parameters that affect the permeabilization of cell membrane by altering squeezing ratio and deformation rate experienced by cells, and therefore inducing different secretion amount of sEVs. To investigate how the gap height affects sEV secretion from BM-MSCs, the devices with different ridge gaps were fabricated. As shown in Fig. 2A, the squeezing ratio is defined as the percentage reduction in cell diameter due to the compression if cell diameter $\geq$ gap height, while squeezing ratio is 0% if cell diameter $<$ gap height (more details described in the Supplementary information section S5). The gap height was fabricated to 17.5 μm, 9.9 μm, 8.0 μm, 6.3 μm, and 5.2 μm, corresponding to the squeezing ratio of 0%–3%, 30%–45%, 43%–56%, 55%–65%, 63%–71%, respectively, taking most cells are of 14–18 μm in diameter. BM-MSCs with a concentration of 2×10^6 cells/mL were introduced into SEED, while the flow velocity of the sample fluid under the squeezing ridges was maintained at 200 mm/s by adjusting the input flow rates. Thereafter, the stimulated BM-MSCs were collected from the device outlet and re-cultured for 48 h in a T25 cell culture flask at a cell seeding number of 5×10^5.

The sEVs secreted from BM-MSCs treated by different SEED devices were then characterized by nano-flow cytometry (NanoFCM) analysis.

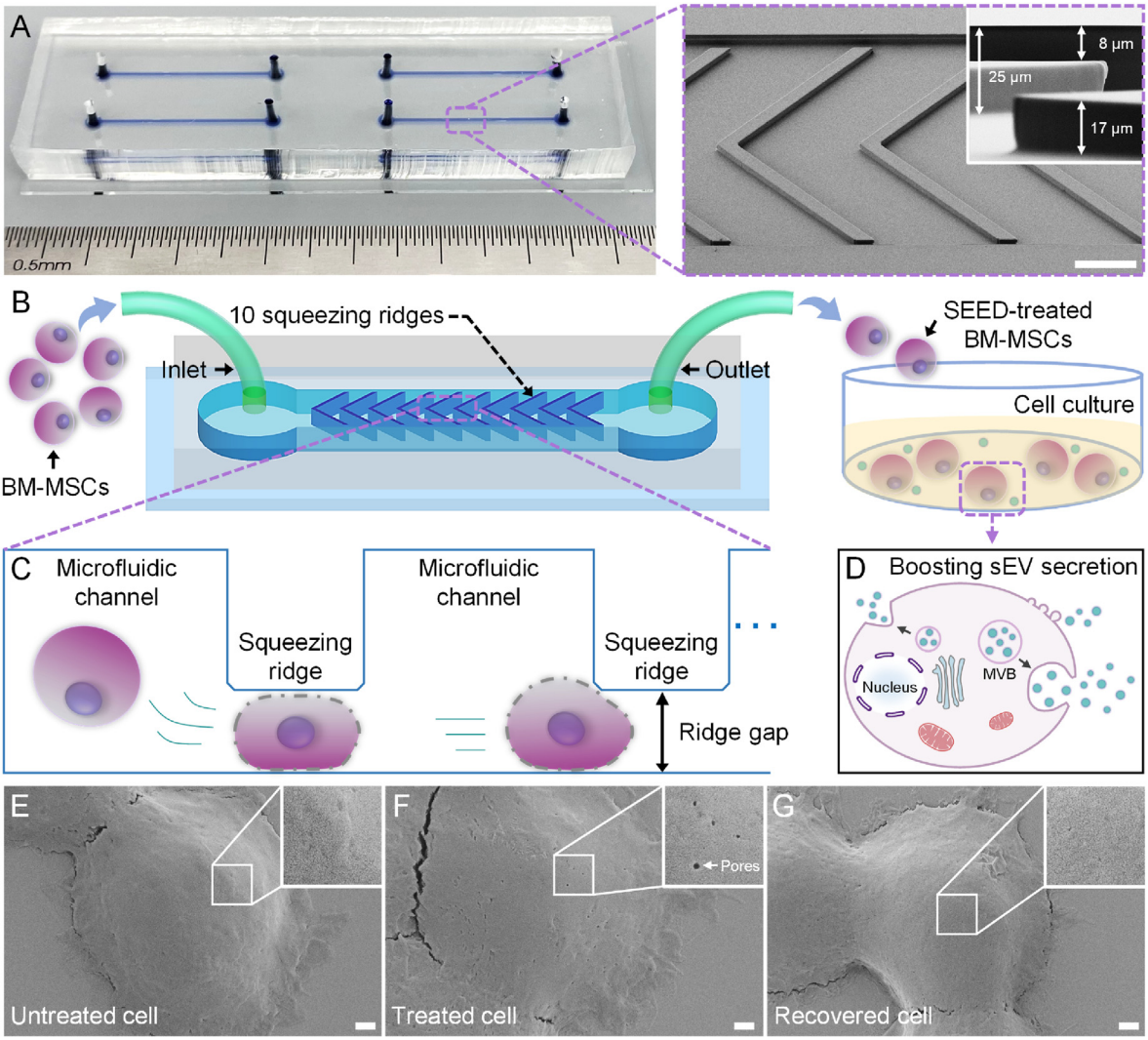

Fig. 1. Picture and schematic illustration of SEED to promote sEV secretion from BM-MSCs by mechanical stimulation. (A) Photograph of the device integrating with four identical microfluidic channels. The insets show scanning electron micrographs on the fishbone-shaped ridges (17 μm in height and 8 μm in gap) inside the channel with height of 25 μm (scale bar: 100 μm). (B) Schematic illustration of the device layout and experimental set-up. BM-MSCs are introduced into SEED through the inlet and then collected at the device outlet, the treated MSCs are re-cultured to isolate sEVs. (C, D) Working principle of SEED to stimulate BM-MSCs to promote sEV secretion. While BM-MSCs rapidly pass through the microfluidic channel with 10 ridge gaps smaller than cell diameter, they take repeated mechanical compression from the squeezing ridges, resulting in transient cell membrane permeabilization. As the treated BM-MSCs are re-cultured, the permeabilization of cell membrane promote cells to secrete more sEVs. (E-G) SEM images of (E) untreated, (F) SEED-treated, and (G) recovered BM-MSCs (scale bars: 1 μm).

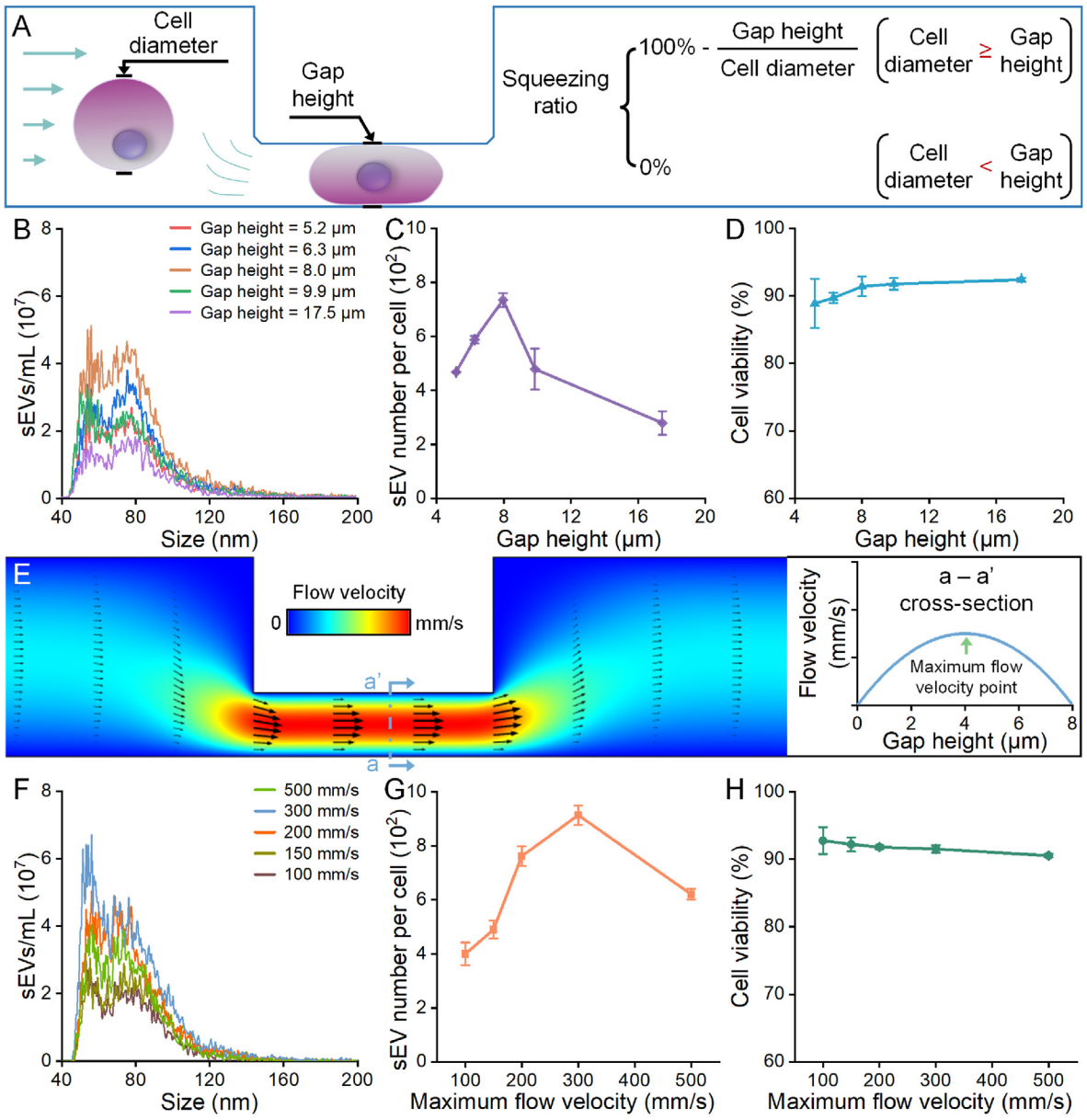

Fig. 2. Enhancement of sEV secretion from BM-MSCs by SEED. (A) Schematic illustration on cell squeezing to define squeezing ratio. (B) Representative size distributions of sEVs isolated from BM-MSCs treated by different SEED devices with gap heights of 5.2 μm, 6.3 μm, 8.0 μm, 9.9 μm, and 17.5 μm, respectively. (C) sEV number per cell produced by SEED-treated BM-MSCs at different gap heights. (D) Plot of cell viability after re-culturing for 48 h as a function of the gap height. (E) FEA simulation of flow filed distribution in the microfluidic channel to illustrate the maximum flow velocity. (F) Size distributions of sEVs isolated from BM-MSCs treated by SEED at maximum flow velocities of 100 mm/s, 150 mm/s, 200 mm/s, 300 mm/s, and 500 mm/s, respectively. (G) sEV number per cell produced by SEED-treated BM-MSCs at different maximum flow velocities. (H) Plot of cell viability after re-culturing for 48 h as a function of maximum flow velocity. All error bars represent mean ± standard error of the mean (N = 3 devices).

Size distribution of sEVs secreted by stimulated BM-MSCs has a similar pattern and an approximate size range of 40–200 nm (Fig. 2B). Nevertheless, sEV secretion amount is associated with ridge gap, as shown in Fig. 2C. When the gap height is decreased from 17.5 μm to 8.0 μm, the average sEV number secreted by each BM-MSC is improved, and the largest secretion amount is obtained at the gap height of 8.0 μm, which therefore is the optimal gap height to be used in subsequent experiments. It has been demonstrated that gap height is negatively correlated to compression strength [45], the compression can increase permeabilization of cell membrane and stimulate cells to secrete more sEVs [29]. However, when gap height is decreased from 8.0 μm to 5.2 μm, a reversed trend appears, which is caused by detrimental effects of mechanical stimulation on cell viability, excessive compression strength leads to a decrease in the secretion amount of sEVs from BM-MSCs (Fig. 2D).

Next, flow velocity on sEV secretion was further assessed using SEED with gap height of 8.0 μm. As shown in Fig. 2E, FEA was performed to investigate flow field distribution in the microfluidic channel (more details presented in Materials and methods). The flow velocity field shows a parabolic profile along the depth direction of the ridge gap and the maximum flow velocity is located at the apex of the curve. By adjusting input flow rates at the device inlet, BM-MSCs were mechanically deformed as they passed through the ridge gaps at different maximum flow velocities of 100 mm/s, 150 mm/s, 200 mm/s, 300 mm/s, and 500 mm/s, respectively. NanoFCM results suggest that increasing the maximum flow velocity from 100 mm/s to 300 mm/s results in a higher

secretion amount of sEVs, while not changing their size distribution pattern, as shown in Fig. 2F and G. However, when the maximum flow velocity exceeds 300 mm/s, ultrafast cell deformation also leads to a decrease in cell viability (Fig. 2H), thereby reducing the secretion amount of sEVs from BM-MSCs. According to the abovementioned results, gap height of 8.0 μm (i.e., squeezing ratio ≈ 43%–56%) and maximum flow velocity of 300 mm/s are the optimal operating parameters for promoting sEV secretion from BM-MSCs, and they were then used in the following studies.

3.3. Characterization of BM-MSCs and sEVs

Since yield and properties of sEVs are regulated by cell status [7,46], the effects of mechanical squeezing on morphology, growth rate, viability and stemness of BM-MSCs were then investigated after optimizing experimental parameters of SEED. For comparison, cells of control group were incubated in medium but not treated by the device, followed by re-culturing in a T25 cell culture flask at the same cell-seeding density for 48 h. As show in Fig. 3A, BM-MSCs treated by SEED (i.e., SEED group) present a fibroblast-like spindle-shaped appearance, and their morphology is consistent with the untreated cells (i.e., control group). Both SEED-treated and untreated BM-MSCs grow normally in culture flasks, reaching approximately 80%–90% confluence throughout the culture period. Afterwards, BM-MSCs were collected from culture flasks and characterized using a trypan blue exclusion test (more details presented in Materials and methods). Growth rates of BM-MSCs in two groups are statistically similar (Fig. 3B), indicating that the cell viability of BM-MSCs is not affected by mechanical squeezing under the optimal condition (Fig. 3C). Further, in order to evaluate the stemness of SEED-treated BM-MSCs, the collected cells were also tested by flow cytometry on their expression of MSC-associated cell surface markers (more details presented in Materials and methods). SEED-treated and untreated BM-MSCs show (Fig. 3D) a positive rate over 95% for CD44, CD73, and CD105, as well as a negative rate less than 2% for CD11b, CD34, and CD45, which are in agreement with previous report [38]. Moreover, there is no statistically significant difference in surface marker expression between the two groups of cells.

Furthermore, sEVs secreted from BM-MSCs upon mechanical stimulation were investigated by characterizing their membrane morphology, protein markers, particle number, size distribution, and miRNA content. Transmission electron microscopy (TEM) shows that the nanoparticles isolated from both SEED-treated and untreated BM-MSCs present a clear membrane structure with cup-shaped or saucer-like morphology, the results are in accordance with sEVs (Fig. 4A and B) [36]. It also confirms that the topography of sEVs is not changed by SEED treatment. Western blot analysis was preformed to identify the protein markers of the isolated nanoparticles. As shown in Fig. 4C, both groups of nanoparticles are positive for sEV-specific markers CD81, CD9, and TSG101, and negative for endoplasmic reticulum marker Calnexin, identifying them as sEVs [3,47].

Thereafter, particle number and size distribution of sEVs isolated from both SEED-treated and untreated BM-MSCs were measured by NanoFCM. As shown in Fig. 4D, each SEED-treated BM-MSC secretes on average ~914 sEVs, while each untreated cell secretes on average ~234 sEVs, demonstrating that SEED can lead to approximate 4-fold increase in the secretion amount of sEVs. This enhancement on sEV secretion was also checked by protein quantification analysis (Fig. 4E). Although both groups of sEVs show a similar size range of 40–200 nm, their size distributions are slightly different (Fig. 4F). Compared to the control group, the proportion of sEVs derived from the SEED group in the size range of 40–80 nm is increased from 51% to 64%, while the proportion of sEVs with larger size is accordingly decreased (Fig. 4G). Furthermore, the miRNA content of sEVs secreted by both SEED-treated and untreated BM-MSCs were characterized by RT-qPCR, eight key miRNAs involving in corneal epithelial wound healing were analyzed, including hsa-miR-21-5p, hsa-miR-138-5p, hsa-miR-106a-5p, hsa-miR-99b-3p, hsa-miR-19b-3p, hsa-miR-28-5p, hsa-miR-24-3p, and hsa-miR-151a-3p [48–50]. As shown in Fig. 4H, the gene expression of all miRNAs is not or minimally altered by the SEED treatment, and there is no statistically significant difference in miRNA levels between the two groups of sEVs.

3.4. Cellular uptake of SEED-induced sEVs

Non-retinal-derived adult stem cells, such as BM-MSCs, have been widely studied for eye therapies, and have drawn much attention as an alternative modality in the management of corneal diseases [51,52]. The therapeutic effects of MSCs are widely mediated by MSCs differentiation and paracrine signaling via EVs [53]. Therefore, here we used immortalized human corneal epithelial cells (iHCECs) and established a corneal epithelial wound model in the next section to evaluate the SEED-induced sEVs.

The sEV uptake by iHCECs was evaluated by observing cellular

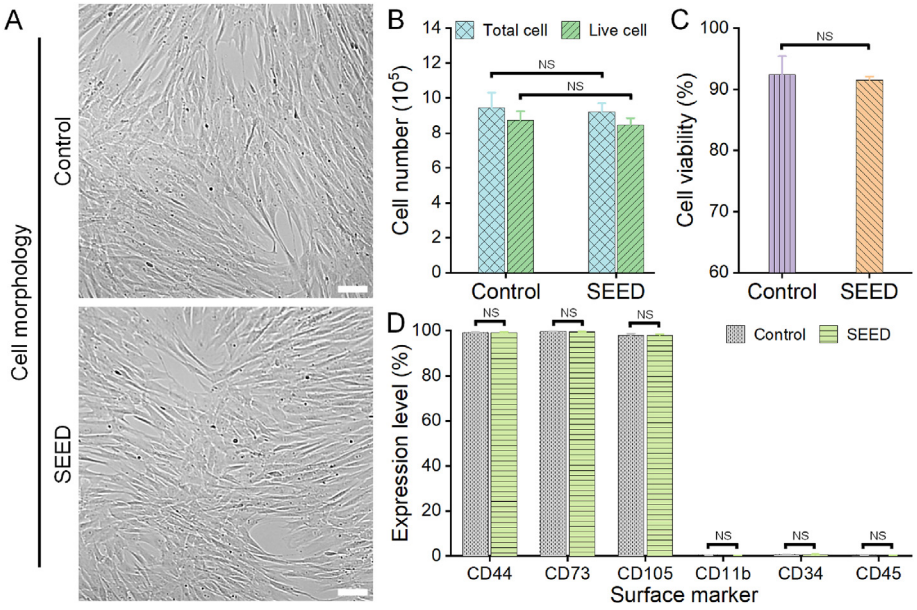

Fig. 3. Characterization of BM-MSCs. (A) Cell morphology of untreated (Control) and SEED-treated (SEED) BM-MSCs after re-culturing for 48 h (scale bars: 100 μm). (B) Number of total and live cells obtained from different experimental groups. (C) Cell viability of BM-MSCs upon different treatments. (D) Expression of cell surface markers on BM-MSCs untreated and treated by SEED, respectively. CD44, CD73, and CD105 are used as BM-MSC-specific markers, while CD11b, CD34, and CD45 are used as negative markers. All error bars represent mean ± standard error of the mean (N = 3 devices, NS represents no statistical significance).

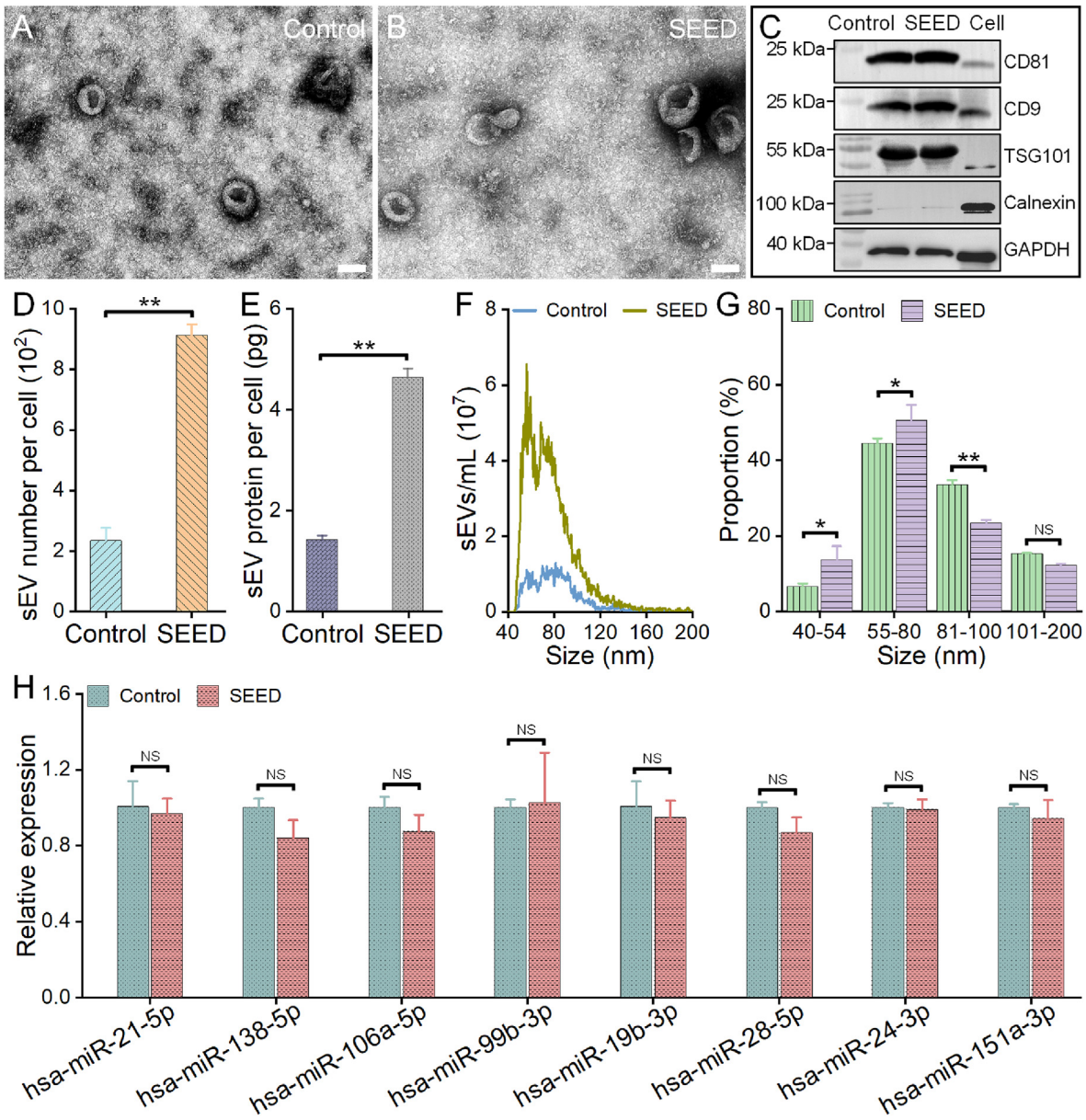

Fig. 4. Characterization of sEVs obtained from different experimental groups. (A, B) TEM images of sEVs secreted by (A) untreated and (B) SEED-treated BM-MSCs (scale bars: 100 nm). (C) Western blot analysis on the protein markers CD81, CD9, TSG101, Calnexin, and GAPDH of sEVs from untreated (left column), SEED-treated (middle column) BM-MSCs, and cell lysate (right column). (D) Number of sEVs secreted by each untreated cell and each SEED-treated cell. (E) Quantification of protein amount in sEVs derived from each untreated cell and each SEED-treated cell. (F) Representative size distribution of sEVs isolated from BM-MSCs that are untreated (Control) and treated by the device (SEED), respectively. (G) Histogram on the size distribution of sEVs isolated from different experimental groups. (H) RT-qPCR analysis on expression levels of miRNAs involving in corneal epithelial wound healing. All error bars represent mean ± standard error of the mean (N = 3 devices, *P < 0.05, **P < 0.01, NS represents no statistical significance).

internalization of SEED-induced sEVs (i.e., SEED group) using fluorescence microscopy (more details presented in Materials and methods), compared with sEVs secreted by untreated BM-MSCs as the control group. In the experiment, sEV samples derived from SEED group (~7.9 × 10^8 sEVs/mL) and control group (~2.0 × 10^8 sEVs/mL) were respectively mixed with a staining working solution prepared by lipophilic fluorescent dye PKH26, followed by an ultracentrifugation step to purify the labeled sEV samples (Fig. 5A). To eliminate background noise, the PKH26 working solution was also processed by the same experimental procedures to set the basal level of residual PKH26 molecules (i.e., background group). Afterwards, 300 μL of sEV sample was added to iHCECs and co-incubated for 14 h. For comparison, labeled sEVs from the SEED group was diluted 4-fold (i.e., dilution group), followed by incubation with iHCECs to determine the influence of mechanical squeezing on sEV uptake. As shown in Fig. 5B, the fluorescent signal of PKH26 dye is observed in the cells co-incubated with PKH26-labeled sEVs, but not in the cells in the background group. Therefore, the sEVs derived from both SEED-treated and untreated BM-MSCs can be taken up efficiently by the iHCECs. Under the same imaging condition (Fig. 5C), the average fluorescent intensity (F.I.) generated by PKH26 molecules in each iHCEC of the SEED group increases approximately 4-fold compared to that from the control group (Fig. 5D), indicating the significant enhancement of the SEED treatment on sEV secretion. Moreover, when the sEV sample derived from SEED-treated BM-MSCs is diluted 4-fold and co-incubated with the iHCECs, the quantification results show that there is no statistically significant difference in the F.I. per cell between the

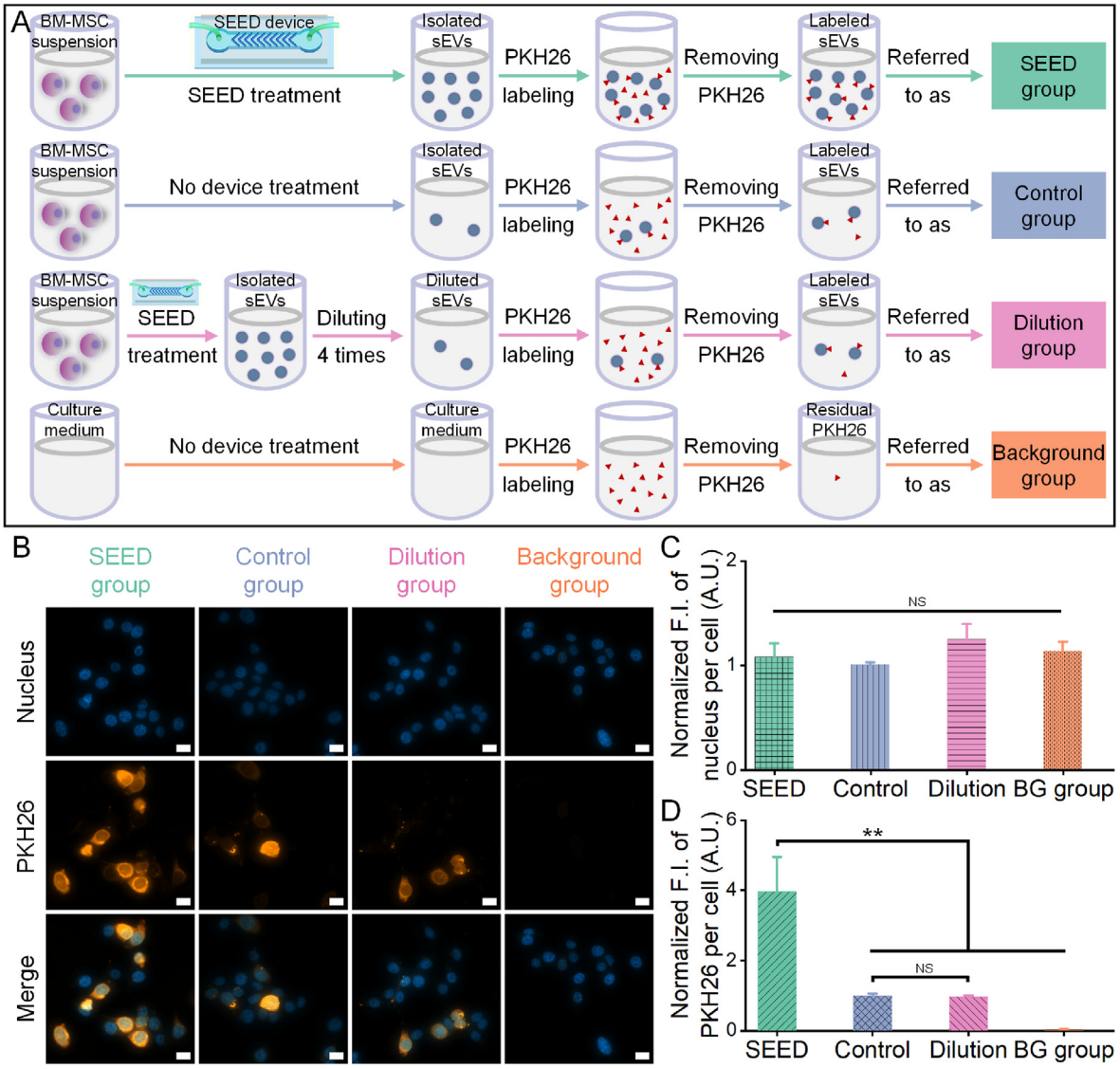

Fig. 5. sEV uptake by iHCECs. (A) Schematic illustration on experimental procedures of labeling sEVs by lipophilic fluorescent dye PKH26. The sEVs are isolated from both SEED-treated (SEED) and untreated (Control) BM-MSCs, while the 4-fold diluted sEV sample from the SEED group is regarded as Dilution group. To eliminate background noise, PKH26 solution with identical dye concentration is processed by the same experimental procedure to set the basal level of residual PKH26 molecules (Background). (B) Fluorescence images on iHCECs (scale bars: 20 μm). SEED (first column), Control (second column), Dilution (third column), and Background (fourth column) represent that iHCECs are co-incubated with the corresponding labeling samples for 14 h, respectively. (C, D) Fluorescent intensity (F.I.) per cell of (C) nucleus and (D) PKH26 quantified from (B), normalized by the intensity of Control group. All error bars represent mean ± standard error of the mean ($N = 3$, $^{**}P < 0.01$, NS represents no statistical significance).

dilution group and the control group, meaning that the uptake amount of PKH26-labeled sEVs into both groups of iHCECs is comparable. These results suggest that mechanical stimulation under the optimal condition does not affect the uptake activity of BM-MSC-secreted sEVs.

3.5. *Effects of SEED-induced sEVs on corneal epithelial wound healing in vitro*

sEVs derived from MSCs have been widely used to promote tissue repair, such as corneal wound healing, lung injury therapy, fracture healing, liver fibrosis regression, etc., therefore showing promising regenerative capability [8,17,52]. To investigate whether mechanical treatment by SEED affected the functionalities of sEVs, an *in vitro* scratch closure assay on corneal epithelial cells was performed (Fig. 6A). A confluent monolayer of iHCECs was scraped using a scratcher with tip size of 1 mm, and then co-incubated with sEV samples isolated from both SEED-treated BM-MSCs (i.e., SEED group) and untreated BM-MSCs (i.e., control group), 4-fold diluted sEV sample from the SEED group (i.e., dilution group), and serum-free DMEM/F-12 medium (i.e., medium group) for 0–30 h, respectively (more details presented in Materials and methods). As shown in Fig. 6B, the edges of scratch wounds at different time points are accurately traced with red lines through image processing to obtain wound areas. Compared to the cells treated by culture medium, sEVs secreted by BM-MSCs can effectively enhance the migration ability of iHCECs (Fig. 6C). Since the BM-MSCs treated by SEED can secrete more sEVs, the corneal epithelial wound in the SEED group heals faster than other groups. When the wound area of iHCEC monolayer heals from $\sim 10 \times 10^5$ μm^2 (starting point of the scratch closure assay) to $\sim 7 \times 10^5$ μm^2, the incubation time of the control group requires 30 h, while the SEED group takes only 16 h. It is worth noting that when corneal epithelial wounds are co-incubated with 4-fold diluted sEV sample obtained from the SEED group, the wound closure rate and migration area

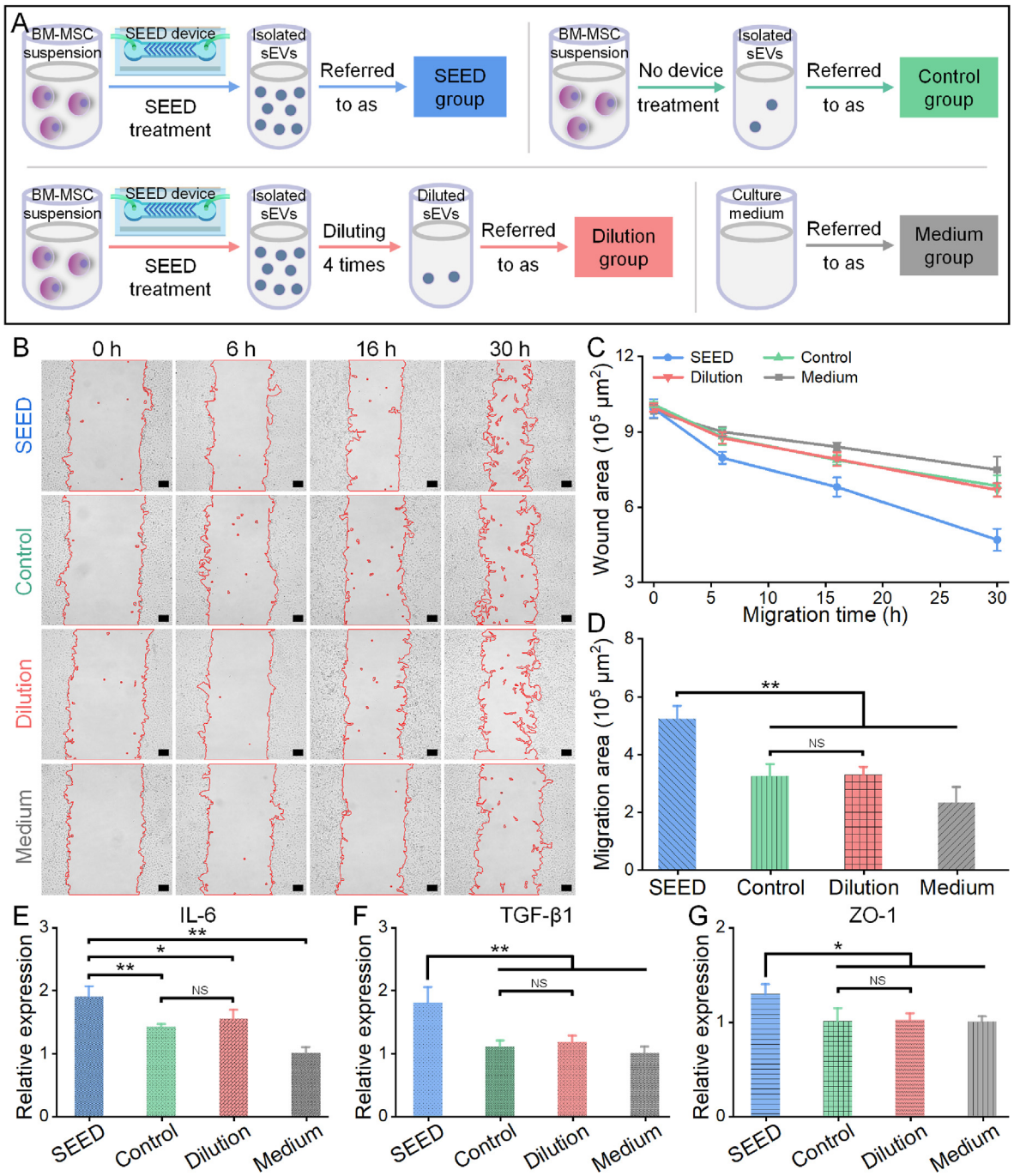

Fig. 6. Effects of BM-MSC-derived sEVs on scratch closure healing of iHCECs. (A) Schematic illustration of experimental procedures on collecting sEV samples. The sEV are secreted by both SEED-treated (SEED) and untreated (Control) BM-MSCs, while the 4-fold diluted sEV sample from the SEED group is regarded as Dilution group. Medium group represents using same volume of serum-free culture medium. (B) Microscopic images on the scratch wound of iHCECs after incubating with abovementioned samples for 0 h (first column), 6 h (second column), 16 h (third column), and 30 h (fourth column), respectively (scale bars: 100 μm). (C, D) Wound area and migration area quantified from (B). (E-G) RT-qPCR analysis on mRNA expression levels of cytokines IL-6 (E), TGF-β1 (F), ZO-1 (G). All error bars represent mean ± standard error of the mean (N = 3, *P < 0.05, **P < 0.01, NS represents no statistical significance).

of iHCECs are comparable to those of the control group (Fig. 6C and D), indicating that SEED does not alter the bioactivity of BM-MSC-secreted sEVs. Following the scratch wound healing, the effects of BM-MSC-secreted sEVs on gene expression of cytokines related to the corneal epithelial wound repair were further analyzed. As shown in Fig. 6E–G, the scratched iHCEC monolayer treated by the sEVs derived from the SEED group shows an upregulation of IL-6, TGF-β1, and ZO-1 genes compared to other groups, which is consistent with previously works on the corneal wound healing [52,54]. Due to their immunoregulatory mechanism, the upregulated mRNA IL-6 and mRNA TGF-β1 can help to repair corneal epithelial damage and restore tight junctional barrier function. Moreover, the increase in mRNA ZO-1 expression also confirms that the enhancement of sEV secretion stimulated by SEED is conducive to repair barrier function of the tight epithelial junction. Meanwhile, there is no statistically significant difference in the expression of the above three mRNAs between the dilution group and the

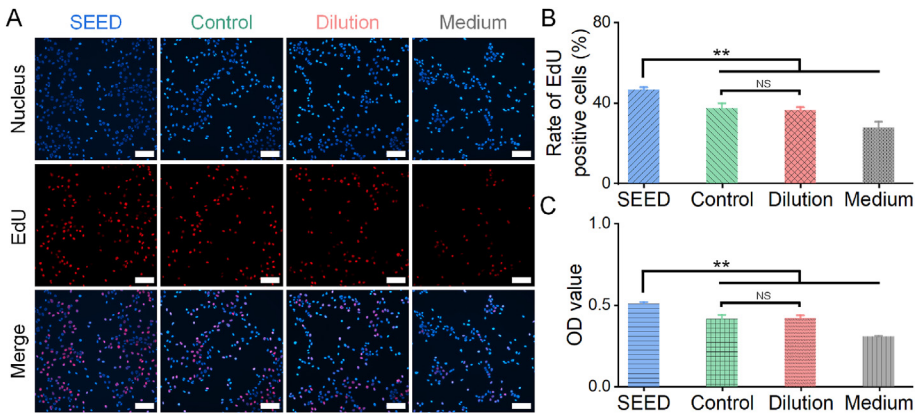

Fig. 7. Effects of BM-MSC-derived sEVs on proliferation of iHCECs. (A) EdU analysis on iHCECs after co-incubation with sEV sample derived from SEED-treated BM-MSCs (SEED), sEV sample isolated from untreated BM-MSCs (Control), 4-fold diluted sEV sample from the SEED group (Dilution), and serum-free DMEM/F-12 (Medium), respectively, for 18 h (scale bars: 100 μm). (B) Rate of EdU positive cells quantified from (A) by cell counting. (C) Cell proliferation of iHCECs quantified by CCK-8 assays after co-incubation with different samples. All error bars represent mean ± standard error of the mean (N = 3, $^{**}P < 0.01$, NS represents no statistical significance).

control group, indicating that the mechanical stimulation by SEED does not alter the bioactivity of BM-MSC-secreted sEVs in regulating the gene expression of IL-6, TGF-β1, and ZO-1.

Furthermore, the ability of sEVs derived from BM-MSCs to promote iHCEC proliferation was assessed by 5-ethynyl-2′-deoxyuridine (EdU) analysis (more details presented in Materials and methods). As shown in Fig. 7A, the number of EdU-labeled iHCECs is higher in SEED, control, and dilution groups compared to that of the medium group, indicating the enhancement of BM-MSC-secreted sEVs on iHCEC proliferation. Quantitatively, the rates of EdU positive cells (EdU-labeled cells as a percentage of total cells) in the abovementioned three groups are 46.5%, 37.3%, and 36.3%, respectively (Fig. 7B). Since SEED can stimulate BM-MSCs to secrete more sEVs, iHCECs proliferation in the SEED group is higher than that in the control group. Moreover, there is no statistically significant difference in the rate of EdU positive cells between the dilution group and the control group, indicating that SEED does not alter the bioactivity of BM-MSC-secreted sEVs in enhancing cell proliferation. In addition, a CCK-8 assay was also performed to check the enhancement effect by BM-MSC-secreted sEVs on proliferation of iHCECs (more details presented in Materials and methods), similar experimental results were also found (Fig. 7C). Taken together, the abovementioned scratch closure, RT-qPCR, EdU, CCK-8 assays all demonstrate that mechanical squeezing under the optimal condition does not affect the functionality of BM-MSC-secreted sEVs, therefore promoting corneal epithelial wound healing and indicating potential applications of this technique.

4. Discussion

In the past decade, microfluidic cell squeezing method has been developed into one of the leading techniques for cell therapy [33], representative works include cell squeezing devices [31], cell deformation chips [55], cell volume exchange for convective transfer platforms [43], cell hydroporators [56], etc. In this technique, as cells rapidly pass through a microfluidic confinement, mechanical stress triggers rearrangement of lipid molecules, thereby introducing transient nanopores on cell membrane [32,57]. Currently, such technology has been advanced into clinical trials (no. NCT04084951), generating engineered cell vaccines for cancer immunotherapy *ex vivo* [58,59]. Despite the considerable achievements in the disease treatment, the studies on microfluidic mechanical squeezing were primarily used for intracellular delivery of various exogenous cargos. In order to expand the application fields of this technology and deliver a novel method, we have developed a microfluidic device that can effectively stimulate BM-MSCs to secrete more sEVs. Similar to the working mechanism of electrical stimulation and acoustic excitation, cell membranes are permeabilized by mechanical effect to generate transient nanopores (Fig. 1F), allowing influx of Ca^{2+} into cytosol to stimulate sEV secretion of cells [9,15,23,29]. According to the stimulation principle of cell membrane disruption, theoretically, SEED-induced sEV secretion is independent of cell sources, and therefore can be applicable across a variety of cells with narrow size distribution, as long as the cell diameter is larger than the height of ridge gap in the microfluidic channel [31,43].

Unlike to biochemical methods to improve sEV secretion, the microfluidic mechanical squeezing platform does not require biological or chemical additives, avoiding altering the physiological functions of the donor cells and their secreted sEVs [15]. In addition, SEED was developed by microfluidic technology, enabling localization of mechanical squeezing to the cellular scale and thus achieving more precise and homogeneous physical stimulation [26]. Moreover, since no external electric field is required, this technique can effectively avoid cell damage caused by metal contamination, Joule heating, and pH changes [28]. As presented in the experimental results, mechanical stimulation under the optimal condition does not alter the viability and stemness of BM-MSCs, and the secretion mount of sEVs from SEED-treated BM-MSCs is significantly increased compared to the untreated cells, therefore accelerating *in vitro* corneal epithelial wound healing. In future, this technique could cooperate with the mechanical cell deformation platforms for intracellular delivery. In this case, by microfluidic cell squeezing, a variety of exogenous cargos can be loaded into the cells, and the mechanical stimulation can also boost the cells to secrete more sEVs, thereby generation of more cargo-carrying sEVs could be envisaged, the latter as smart cargo carrier for intracellular delivery holds great potential for therapeutics due to their low immunogenicity, affordable cost, etc. [7,60,61] Moreover, with the advantage of microfluidic cell squeezing technique in intracellular delivery of exogenous cargos with large size, such as mRNA, plasmid DNA, nanomaterials, etc. [33,62], the SEED platform is also expected to address the technical challenges of limited cargo size and low loading efficiency faced by current sEV loading studies [29,63].

5. Conclusion

In this work, we have presented a microfluidic device to improve sEV secretion from BM-MSCs. Rapid mechanical disruption transiently permeabilizes cell membrane, thereby stimulating cells to secrete more sEVs into extracellular environment, while not negatively interfering cellular growth state. Under optimal experimental conditions, the average amount of sEVs secreted by each SEED-treated BM-MSC can reach approximately 10^3, increased about 4-fold compared to untreated cells. Characterization of cells and sEVs also confirmed that mechanical stimulation presented here does not affect the functionality of BM-MSC-induced sEVs, they can be efficiently taken up by iHCECs and effectively accelerate corneal epithelial wound healing *in vitro*. Therefore, the microfluidic mechanical squeezing is an effective stimulation method for boosting sEV secretion and the SEED is expected to evolve into a robust and versatile tool to improve sEV yield for biomedical applications.

Credit author statement

H.Y. Conceived the study. H.Y. and H.G. Supervised the project. R.H., S.H., and H.Y. Designed the experiments. R.H., S.H., H.Z., X.C., Z.Y., and J.R. Performed the experiments. R.H., S.H., H.Y., H.Z., and X.C. analyzed the experimental results. R.H. and H.Y. Wrote the manuscript. H.Y. and H.G. Discussed and edited the manuscript.

Declaration of competing interest

The authors declare that they have no known competing financial interests or personal relationships that could have appeared to influence the work reported in this paper.

Data availability

The data that support the findings of this study are available from the corresponding author upon reasonable request.

Acknowledgements

This work was financially supported by the National Natural Science Foundation of China (grant numbers 62074155, 62175252), Guangdong Basic and Applied Basic Research Foundation (grant numbers 2020A1515110938, 2020A1515110142), Shenzhen Science and Technology Innovation Commission (grant numbers KCXFZ2020020110081240, JCYJ20210324101405016). The authors also thank Zengrong Fan, Dr. Pengcheng Zhang, Dr. Lin Zeng, Dr. Guoqiang Gu, and Sihui Chen for discussion and assistance on the experiments.

Appendix A. Supplementary data

Supplementary data to this article can be found online at https://doi.org/10.1016/j.mtbio.2022.100527.

References

[1] C. Théry, K.W. Witwer, E. Aikawa, M.J. Alcaraz, J.D. Anderson, R. Andriantsitohaina, A. Antoniou, T. Arab, F. Archer, G.K. Atkin-Smith, D.C. Ayre, J.M. Bach, D. Bachurski, H. Baharvand, L. Balaj, S. Baldacchino, N.N. Bauer, A.A. Baxter, M. Bebawy, C. Beckham, A. Bedina Zavec, A. Benmoussa, A.C. Berardi, P. Bergese, E. Bielska, C. Blenkiron, S. Bobis-Wozowicz, E. Boilard, W. Boireau, A. Bongiovanni, F.E. Borràs, S. Bosch, C.M. Boulanger, X. Breakefield, A.M. Breglio, M.Á. Brennan, D.R. Brigstock, A. Brisson, M.L. Broekman, J.F. Bromberg, P. Bryl-Górecka, S. Buch, A.H. Buck, D. Burger, S. Busatto, D. Buschmann, B. Bussolati, E.I. Buzás, J.B. Byrd, G. Camussi, D.R. Carter, S. Caruso, L.W. Chamley, Y.T. Chang, C. Chen, S. Chen, L. Cheng, A.R. Chin, A. Clayton, S.P. Clerici, A. Cocks, E. Cocucci, R.J. Coffey, A. Cordeiro-da-Silva, Y. Couch, F.A. Coumans, B. Coyle, R. Crescitelli, M.F. Criado, C. D'Souza-Schorey, S. Das, A. Datta Chaudhuri, P. de Candia, E.F. De Santana Junior, O. De Wever, H.A. del Portillo, T. Demaret, S. Deville, A. Devitt, B. Dhondt, D. Di Vizio, L.C. Dieterich, V. Dolo, A.P. Dominguez Rubio, M. Dominici, M.R. Dourado, T.A. Driedonks, F.V. Duarte, H.M. Duncan, R.M. Eichenberger, K. Ekström, S. EL Andaloussi, C. Elie-Caille, U. Erdbrügger, J.M. Falcón-Pérez, F. Fatima, J.E. Fish, M. Flores-Bellver, A. Försönits, A. Frelet-Barrand, F. Fricke, G. Fuhrmann, S. Gabrielsson, A. Gámez-Valero, C. Gardiner, K. Gärtner, R. Gaudin, Y.S. Gho, B. Giebel, C. Gilbert, M. Gimona, I. Giusti, D.C. Goberdhan, A. Görgens, S.M. Gorski, D.W. Greening, J.C. Gross, A. Gualerzi, G.N. Gupta, D. Gustafson, A. Handberg, R.A. Haraszti, P. Harrison, H. Hegyesi, A. Hendrix, A.F. Hill, F.H. Hochberg, K.F. Hoffmann, B. Holder, H. Holthofer, B. Hosseinkhani, G. Hu, Y. Huang, V. Huber, S. Hunt, A.G.E. Ibrahim, T. Ikezu, J.M. Inal, M. Isin, A. Ivanova, H.K. Jackson, S. Jacobsen, S.M. Jay, M. Jayachandran, G. Jenster, L. Jiang, S.M. Johnson, J.C. Jones, A. Jong, T. Jovanovic-Talisman, S. Jung, R. Kalluri, S.I. Kano, S. Kaur, Y. Kawamura, E.T. Keller, D. Khamari, E. Khomyakova, A. Khvorova, P. Kierulf, K.P. Kim, T. Kislinger, M. Klingeborn, D.J. Klinke II, M. Kornek, M.M. Kosanović, Á.F. Kovács, E.M. Krämer-Albers, S. Krasemann, M. Krause, I.V. Kurochkin, G.D. Kusuma, S. Kuypers, S. Laitinen, S.M. Langevin, L.R. Languino, J. Lannigan, C. Lässer, L.C. Laurent, G. Lavieu, E. Lázaro-Ibáñez, S. Le Lay, M.S. Lee, Y.X.F. Lee, D.S. Lemos, M. Lenassi, A. Leszczynska, I.T. Li, K. Liao, S.F. Libregts, E. Ligeti, R. Lim, S.K. Lim, A. Linē, K. Linnemannstöns, A. Llorente, C.A. Lombard, M.J. Lorenowicz, Á.M. Lörincz, J. Lötvall, J. Lovett, M.C. Lowry, X. Loyer, Q. Lu, B. Lukomska, T.R. Lunavat, S.L. Maas, H. Malhi, A. Marcilla, J. Mariani, J. Mariscal, E.S. Martens-Uzunova, L. Martin-Jaular, M.C. Martinez, V.R. Martins, M. Mathieu, S. Mathivanan, M. Maugeri, L.K. McGinnis, M.J. McVey, D.G. Meckes Jr., K.L. Meehan, I. Mertens, V.R. Minciacchi, A. Möller, M. Møller Jørgensen, A. Morales-Kastresana, J. Morhayim, F. Mullier, M. Muraca, L. Musante, V. Mussack, D.C. Muth, K.H. Myburgh, T. Najrana, M. Nawaz, I. Nazarenko, P. Nejsum, C. Neri, T. Neri, R. Nieuwland, L. Nimrichter, J.P. Nolan, E.N. Nolte-'t Hoen, N. Noren Hooten, L. O'Driscoll, T. O'Grady, A. O'Loghlen, T. Ochiya, M. Olivier, A. Ortiz, L.A. Ortiz, X. Osteikoetxea, O. Østergaard, M. Ostrowski, J. Park, D.M. Pegtel, H. Peinado, F. Perut, M.W. Pfaffl, D.G. Phinney, B.C. Pieters, R.C. Pink, D.S. Pisetsky, E. Pogge von Strandmann, I. Polakovicova, I.K. Poon, B.H. Powell, I. Prada, L. Pulliam, P. Quesenberry, A. Radeghieri, R.L. Raffai, S. Raimondo, J. Rak, M.I. Ramirez, G. Raposo, M.S. Rayyan, N. Regev-Rudzki, F.L. Ricklefs, P.D. Robbins, D.D. Roberts, S.C. Rodrigues, E. Rohde, S. Rome, K.M. Rouschop, A. Rughetti, A.E. Russell, P. Saá, S. Sahoo, E. Salas-Huenuleo, C. Sánchez, J.A. Saugstad, M.J. Saul, R.M. Schiffelers, R. Schneider, T.H. Schøyen, A. Scott, E. Shahaj, S. Sharma, O. Shatnyeva, F. Shekari, G.V. Shelke, A.K. Shetty, K. Shiba, P.R.M. Siljander, A.M. Silva, A. Skowronek, O.L. Snyder II, R.P. Soares, B.W. Sódar, C. Soekmadji, J. Sotillo, P.D. Stahl, W. Stoorvogel, S.L. Stott, E.F. Strasser, S. Swift, H. Tahara, M. Tewari, K. Timms, S. Tiwari, R. Tixeira, M. Tkach, W.S. Toh, R. Tomasini, A.C. Torrecilhas, J.P. Tosar, V. Toxavidis, L. Urbanelli, P. Vader, B.W. van Balkom, S.G. van der Grein, J. Van Deun, M.J. van Herwijnen, K. Van Keuren-Jensen, G. van Niel, M.E. van Royen, A.J. van Wijnen, M.H. Vasconcelos, I.J. Vechetti Jr., T.D. Veit, L.J. Vella, É. Velot, F.J. Verweij, B. Vestad, J.L. Viñas, T. Visnovitz, K.V. Vukman, J. Wahlgren, D.C. Watson, M.H. Wauben, A. Weaver, J.P. Webber, V. Weber, A.M. Wehman, D.J. Weiss, J.A. Welsh, S. Wendt, A.M. Wheelock, Z. Wiener, L. Witte, J. Wolfram, A. Xagorari, P. Xander, J. Xu, X. Yan, M. Yáñez-Mó, H. Yin, Y. Yuana, V. Zappulli, J. Zarubova, V. Žėkas, J.Y. Zhang, Z. Zhao, L. Zheng, A.R. Zheutlin, A.M. Zickler, P. Zimmermann, A.M. Zivkovic, D. Zocco, E.K. Zuba-Surma, Minimal information for studies of extracellular vesicles 2018 (MISEV2018): a position statement of the International Society for Extracellular Vesicles and update of the MISEV2014 guidelines, J. Extracell. Vesicles 7 (2018), 1535750, https://doi.org/10.1002/0471143030.cb0322s30.

[2] A. Möller, R.J. Lobb, The evolving translational potential of small extracellular vesicles in cancer, Nat. Rev. Cancer 20 (2020) 697–709, https://doi.org/10.1038/s41568-020-00299-w.

[3] Y. Ji, W. Han, X. Fu, J. Li, Q. Wu, Y. Wang, Improved small extracellular vesicle secretion of rat adipose-derived stem cells by microgrooved substrates through upregulation of the ESCRT-III-associated protein Alix, Adv. Healthcare Mater. 10 (2021), 2100492, https://doi.org/10.1002/adhm.202100492.

[4] H. Shao, H. Im, C.M. Castro, X. Breakefield, R. Weissleder, H. Lee, New technologies for analysis of extracellular vesicles, Chem. Rev. 118 (2018) 1917–1950, https://doi.org/10.1021/acs.chemrev.7b00534.

[5] N. Ludwig, J.H. Azambuja, A. Rao, D.G. Gillespie, E.K. Jackson, T.L. Whiteside, Adenosine receptors regulate exosome production, Purinergic Signal. 16 (2020) 231–240, https://doi.org/10.1007/s11302-020-09700-7.

[6] Y. Zha, T. Lin, Y. Li, X. Zhang, Z. Wang, Z. Li, Y. Ye, B. Wang, S. Zhang, J. Wang, Exosome-mimetics as an engineered gene-activated matrix induces in-situ vascularized osteogenesis, Biomaterials 247 (2020), 119985, https://doi.org/10.1016/j.biomaterials.2020.119985.

[7] Z.Y. Feng, Q.Y. Zhang, J. Tan, H.Q. Xie, Techniques for increasing the yield of stem cell-derived exosomes: what factors may be involved? Sci. China Life Sci. 64 (2021) 1325–1341, https://doi.org/10.1007/s11427-021-1997-2.

[8] M. Piffoux, A. Nicolás-Boluda, V. Mulens-Arias, S. Richard, G. Rahmi, F. Gazeau, C. Wilhelm, A.K.A. Silva, Extracellular vesicles for personalized medicine: the input of physically triggered production, loading and theranostic properties, Adv. Drug Deliv. Rev. 138 (2019) 247–258, https://doi.org/10.1016/j.addr.2018.12.009.

[9] T. Fukuta, A. Nishikawa, K. Kogure, Low level electricity increases the secretion of extracellular vesicles from cultured cells, Biochem. Biophys. Rep. 21 (2020), 100713, https://doi.org/10.1016/j.bbrep.2019.100713.

[10] X. Zhu, H. Chen, Y. Zhou, J. Wu, S. Ramakrishna, X. Peng, H.S. Nanda, Y. Zhou, Recent advances in biosensors for detection of exosomes, Curr. Opin. Biomed. Eng. 18 (2021), 100280, https://doi.org/10.1016/j.cobme.2021.100280.

[11] R. Hao, Z. Yu, J. Du, S. Hu, C. Yuan, H. Guo, Y. Zhang, H. Yang, A high-throughput nanofluidic device for exosome nanoporation to develop cargo delivery vehicles, Small 17 (2021), 2102150, https://doi.org/10.1002/smll.202102150.

[12] S. Kwon, S. Shin, M. Do, B.H. Oh, Y. Song, V.D. Bui, E.S. Lee, D.G. Jo, Y.W. Cho, D.H. Kim, J.H. Park, Engineering approaches for effective therapeutic applications based on extracellular vesicles, J. Contr. Release 330 (2021) 15–30, https://doi.org/10.1016/j.jconrel.2020.11.062.

[13] G. Jia, Y. Han, Y. An, Y. Ding, C. He, X. Wang, Q. Tang, NRP-1 targeted and cargo-loaded exosomes facilitate simultaneous imaging and therapy of glioma in vitro and in vivo, Biomaterials 178 (2018) 302–316, https://doi.org/10.1016/j.biomaterials.2018.06.029.

[14] W.M. Usman, T.C. Pham, Y.Y. Kwok, L.T. Vu, V. Ma, B. Peng, Y.S. Chan, L. Wei, S.M. Chin, A. Azad, A.B.L. He, A.Y.H. Leung, M. Yang, N. Shyh-Chang, W.C. Cho, J. Shi, M.T.N. Le, Efficient RNA drug delivery using red blood cell extracellular vesicles, Nat. Commun. 9 (2018) 2359, https://doi.org/10.1038/s41467-018-04791-8.

[15] L.A. Ambattu, S. Ramesan, C. Dekiwadia, E. Hanssen, H. Li, L.Y. Yeo, High frequency acoustic cell stimulation promotes exosome generation regulated by a calcium-dependent mechanism, Commun. Biol. 3 (2020) 553, https://doi.org/10.1038/s42003-020-01277-6.

[16] J. Wang, E.E. Bonacquisti, A.D. Brown, J. Nguyen, Boosting the biogenesis and secretion of mesenchymal stem cell-derived exosomes, Cells 9 (2020) 660, https://doi.org/10.3390/cells9030660.

[17] H. Mansoor, H.S. Ong, A.K. Riau, T.P. Stanzel, J.S. Mehta, G.H.-F. Yam, Current trends and future perspective of mesenchymal stem cells and exosomes in corneal diseases, Int. J. Mol. Sci. 20 (2019) 2853, https://doi.org/10.3390/ijms20122853.
[18] D. Ti, H. Hao, C. Tong, J. Liu, L. Dong, J. Zheng, Y. Zhao, H. Liu, X. Fu, W. Han, LPS-preconditioned mesenchymal stromal cells modify macrophage polarization for resolution of chronic inflammation via exosome-shuttled let-7b, J. Transl. Med. 13 (2015) 308, https://doi.org/10.1186/s12967-015-0642-6.
[19] F. Momen-Heravi, S. Bala, K. Kodys, G. Szabo, Exosomes derived from alcohol-treated hepatocytes horizontally transfer liver specific miRNA-122 and sensitize monocytes to LPS, Sci. Rep. 5 (2015) 9991, https://doi.org/10.1038/srep09991.
[20] M. Hedlund, O. Nagaeva, D. Kargl, V. Baranov, L. Mincheva-Nilsson, Thermal- and oxidative stress causes enhanced release of NKG2D ligand-bearing immunosuppressive exosomes in leukemia/lymphoma T and B cells, PLoS One 6 (2011), e16899, https://doi.org/10.1371/journal.pone.0016899.
[21] H. Pick, E.L. Schmid, A.P. Tairi, E. Ilegems, R. Hovius, H. Vogel, Investigating cellular signaling reactions in single attoliter vesicles, J. Am. Chem. Soc. 127 (2005) 2908–2912, https://doi.org/10.1021/ja044605x.
[22] H.S. Bagheri, M. Mousavi, A. Rezabakhsh, J. Rezaie, S.H. Rasta, A. Nourazarian, Ç.B. Avci, H. Tajalli, M. Talebi, A. Oryan, M. Khaksar, M. Kazemi, S.M. Nassiri, S. Ghaderi, B.G. Bagca, R. Rahbarghazi, E. Sokullu, Low-level laser irradiation at a high power intensity increased human endothelial cell exosome secretion via Wnt signaling, Laser Med. Sci. 33 (2018) 1131–1145, https://doi.org/10.1007/s10103-018-2495-8.
[23] Z. Zhao, L. Qu, T. Shuang, S. Wu, Y. Su, F. Lu, D. Wang, B. Chen, Q. Hao, Low-intensity ultrasound radiation increases exosome yield for efficient drug delivery, J. Drug Deliv. Sci. Technol. 57 (2020), 101713, https://doi.org/10.1016/j.jddst.2020.101713.
[24] S. Guo, L. Debbi, B. Zohar, R. Samuel, R.S. Arzi, A.I. Fried, T. Carmon, D. Shevach, I. Redenski, I. Schlachet, A. Sosnik, S. Levenberg, Stimulating extracellular vesicles production from engineered tissues by mechanical forces, Nano Lett. 21 (2021) 2497–2504, https://doi.org/10.1021/acs.nanolett.0c04834.
[25] H. Kang, Y.-h. Bae, Y. Kwon, S. Kim, J. Park, Extracellular vesicles generated using bioreactors and their therapeutic effect on the acute kidney injury model, Adv. Healthcare Mater. 11 (2022), 2101606, https://doi.org/10.1002/adhm.202101606.
[26] M.P. Stewart, A. Sharei, X. Ding, G. Sahay, R. Langer, K.F. Jensen, In vitro and ex vivo strategies for intracellular delivery, Nature 538 (2016) 183–192, https://doi.org/10.1038/nature19764.
[27] J. Wu, D. Wu, G. Wu, H.P. Bei, Z. Li, H. Xu, Y. Wang, D. Wu, H. Liu, S. Shi, C. Zhao, Y. Xu, Y. He, J. Li, C. Wang, X. Zhao, S. Wang, Scale-out production of extracellular vesicles derived from natural killer cells via mechanical stimulation in a seesaw-motion bioreactor for cancer therapy, Biofabrication 14 (2022), 045004, https://doi.org/10.1088/1758-5090/ac7eeb.
[28] M.P. Stewart, R. Langer, K.F. Jensen, Intracellular delivery by membrane disruption: mechanisms, strategies, and concepts, Chem. Rev. 118 (2018) 7409–7531, https://doi.org/10.1021/acs.chemrev.7b00678.
[29] Z. Yang, J. Shi, J. Xie, Y. Wang, J. Sun, T. Liu, Y. Zhao, X. Zhao, X. Wang, Y. Ma, V. Malkoc, C. Chiang, W. Deng, Y. Chen, Y. Fu, K.J. Kwak, Y. Fan, C. Kang, C. Yin, J. Rhee, P. Bertani, J. Otero, W. Lu, K. Yun, A.S. Lee, W. Jiang, L. Teng, B.Y.S. Kim, L.J. Lee, Large-scale generation of functional mRNA-encapsulating exosomes via cellular nanoporation, Nat. Biomed. Eng. 4 (2020) 69–83, https://doi.org/10.1038/s41551-019-0485-1.
[30] P.E. Boukany, A. Morss, W.C. Liao, B. Henslee, H. Jung, X. Zhang, B. Yu, X. Wang, Y. Wu, L. Li, K. Gao, X. Hu, X. Zhao, O. Hemminger, W. Lu, G.P. Lafyatis, L.J. Lee, Nanochannel electroporation delivers precise amounts of biomolecules into living cells, Nat. Nanotechnol. 6 (2011) 747–754, https://doi.org/10.1038/nnano.2011.164.
[31] A. Sharei, J. Zoldan, A. Adamo, W.Y. Sim, N. Cho, E. Jackson, S. Mao, S. Schneider, M.J. Han, A. Lytton-Jean, P.A. Basto, S. Jhunjhunwala, J. Lee, D.A. Heller, J.W. Kang, G.C. Hartoularos, K.S. Kim, D.G. Anderson, R. Langer, K.F. Jensen, A vector-free microfluidic platform for intracellular delivery, Proc. Natl. Acad. Sci. USA 110 (2013) 2082–2087, https://doi.org/10.1073/pnas.1218705110.
[32] A. Liu, T. Yu, K. Young, N. Stone, S. Hanasoge, T.J. Kirby, V. Varadarajan, N. Colonna, J. Liu, A. Raj, J. Lammerding, A. Alexeev, T. Sulchek, Cell mechanical and physiological behavior in the regime of rapid mechanical compressions that lead to cell volume change, Small 16 (2020), 1903857, https://doi.org/10.1002/smll.201903857.
[33] B. Joo, J. Hur, G.B. Kim, S.G. Yun, A.J. Chung, Highly efficient transfection of human primary T lymphocytes using droplet-enabled mechanoporation, ACS Nano 15 (2021) 12888–12898, https://doi.org/10.1021/acsnano.0c10473.
[34] G. Wang, W. Mao, R. Byler, K. Patel, C. Henegar, A. Alexeev, T. Sulchek, Stiffness dependent separation of cells in a microfluidic device, PLoS One 8 (2013), e75901, https://doi.org/10.1371/journal.pone.0075901.
[35] A. Sharei, R. Poceviciute, E.L. Jackson, N. Cho, S. Mao, G.C. Hartoularos, D.Y. Jang, S. Jhunjhunwala, A. Eyerman, T. Schoettle, R. Langer, K.F. Jensen, Plasma membrane recovery kinetics of a microfluidic intracellular delivery platform, Integr. Biol. 6 (2014) 470–475, https://doi.org/10.1039/c3ib40215k.
[36] C. Théry, S. Amigorena, G. Raposo, A. Clayton, Isolation and characterization of exosomes from cell culture supernatants and biological fluids, Curr. Protoc. Cell Biol. 30 (2006) 3, https://doi.org/10.1002/0471143030.cb0322s30, 22.1-3.22.29.
[37] W. Strober, Trypan blue exclusion test of cell viability, Curr. Protoc. Im. 21 (1997), https://doi.org/10.1002/0471142735.ima03bs21. A.3B.1-A.3B.3.
[38] Z.G. Wang, Z.Y. He, S. Liang, Q. Yang, P. Cheng, A.M. Chen, Comprehensive proteomic analysis of exosomes derived from human bone marrow, adipose tissue, and umbilical cord mesenchymal stem cells, Stem Cell Res. Ther. 11 (2020) 511, https://doi.org/10.1186/s13287-020-02032-8.
[39] L. Mai, G. He, J. Chen, J. Zhu, S. Chen, X. Hou, H. Yang, M. Zhang, Y. Wu, Q. Lin, M. Yang, X. Li, Proteomic analysis of hypoxia-induced senescence of human bone marrow mesenchymal stem cells, Stem Cell. Int. 2021 (2021), 5555590, https://doi.org/10.1155/2021/5555590.
[40] W. Liu, L. Li, Y. Rong, D. Qian, J. Chen, Z. Zhou, Y. Luo, D. Jiang, L. Cheng, S. Zhao, F. Kong, J. Wang, Z. Zhou, T. Xu, F. Gong, Y. Huang, C. Gu, X. Zhao, J. Bai, F. Wang, W. Zhao, L. Zhang, X. Li, G. Yin, J. Fan, W. Cai, Hypoxic mesenchymal stem cell-derived exosomes promote bone fracture healing by the transfer of miR-126, Acta Biomater. 103 (2020) 196–212, https://doi.org/10.1016/j.actbio.2019.12.020.
[41] Y. Cao, Y. Zhang, L. Ma, J. Wang, W. Guo, J. Cheng, G. Hu, S. Fu, J. Liu, Niacin stimulates EPH4EV mammary epithelial cell proliferation and mammary gland development in pubertal mice through activation of AKT/mTOR and ERK1/2 signaling pathways, Cell Tissue Res. 384 (2021) 313–324, https://doi.org/10.1007/s00441-020-03355-x.
[42] Y. Feng, X. Guo, H. Tang, SLC6A8 is involved in the progression of non-small cell lung cancer through the Notch signaling pathway, Ann. Transl. Med. 9 (2021) 264, https://doi.org/10.21037/atm-20-5984.
[43] A. Liu, M. Islam, N. Stone, V. Varadarajan, J. Jeong, S. Bowie, P. Qiu, E.K. Waller, A. Alexeev, T. Sulchek, Microfluidic generation of transient cell volume exchange for convectively driven intracellular delivery of large macromolecules, Mater. Today 21 (2018) 703–712, https://doi.org/10.1016/j.mattod.2018.03.002.
[44] J. Loo, I. Sicher, A. Goff, O. Kim, N. Clary, A. Alexeev, T. Sulchek, A. Zamarayeva, S. Han, M. Calero-Garcia, Microfluidic transfection of mRNA into human primary lymphocytes and hematopoietic stem and progenitor cells using ultra-fast physical deformations, Sci. Rep. 11 (2021), 21407, https://doi.org/10.1038/s41598-021-00893-4.
[45] M.T. Saung, A. Sharei, V.A. Adalsteinsson, N. Cho, T. Kamath, C. Ruiz, J. Kirkpatrick, N. Patel, M. Mino-Kenudson, S.P. Thayer, R. Langer, K.F. Jensen, A.S. Liss, J.C. Love, A size-selective intracellular delivery platform, Small 12 (2016) 5873–5881, https://doi.org/10.1002/smll.201601155.
[46] M. Xu, X. Su, X. Xiao, H. Yu, X. Li, A. Keating, S. Wang, R.C. Zhao, Hydrogen peroxide-induced senescence reduces the wound healing-promoting effects of mesenchymal stem cell-derived exosomes partially via miR-146a, Aging Dis 12 (2021) 102–115, https://doi.org/10.14336/AD.2020.0624.
[47] W. Gao, T. Liang, R. He, J. Ren, H. Yao, K. Wang, L. Zhu, Y. Xu, Exosomes from 3D culture of marrow stem cells enhances endothelial cell proliferation, migration, and angiogenesis via activation of the HMGB1/AKT pathway, Stem Cell Res. 50 (2021), 102122, https://doi.org/10.1016/j.scr.2020.102122.
[48] M. Pomatto, C. Gai, F. Negro, M. Cedrino, C. Grange, E. Ceccotti, G. Togliatto, F. Collino, M. Tapparo, F. Figliolini, T. Lopatina, M.F. Brizzi, G. Camussi, Differential therapeutic effect of extracellular vesicles derived by bone marrow and adipose mesenchymal stem cells on wound healing of diabetic ulcers and correlation to their cargoes, Int. J. Mol. Sci. 22 (2021) 3851, https://doi.org/10.3390/ijms22083851.
[49] J. An, X. Chen, W. Chen, R. Liang, P.S. Reinach, D. Yan, L. Tu, MicroRNA expression profile and the role of miR-204 in corneal wound healing, Invest. Ophthalmol. Vis. Sci. 56 (2015) 3673–3683, https://doi.org/10.1167/iovs.15-16467.
[50] Y.M. Wang, T.K. Ng, K.W. Choy, H.K. Wong, W.K. Chu, C.P. Pang, V. Jhanji, Histological and microRNA signatures of corneal Epithelium in keratoconus, J. Refract. Surg. 34 (2018) 201–211, https://doi.org/10.3928/1081597X-20171215-02.
[51] A.W. Taylor, Ocular immune privilege and transplantation, Front. Immunol. 7 (2016) 37, https://doi.org/10.3389/fimmu.2016.00037.
[52] Z. Yu, R. Hao, J. Du, X. Wu, X. Chen, Y. Zhang, W. Li, Z. Gu, H. Yang, A human cornea-on-a-chip for the study of epithelial wound healing by extracellular vesicles, iScience 25 (2022), 104200, https://doi.org/10.1016/j.isci.2022.104200.
[53] J. Burrello, S. Monticone, C. Gai, Y. Gomez, S. Kholia, G. Camussi, Stem cell-derived extracellular vesicles and immune-modulation, Front. Cell Dev. Biol. 4 (2016) 83, https://doi.org/10.3389/fcell.2016.00083.
[54] J.Y. Oh, M.K. Kim, M.S. Shin, H.J. Lee, J.H. Ko, W.R. Wee, J.H. Lee, The anti-inflammatory and anti-angiogenic role of mesenchymal stem cells in corneal wound healing following chemical injury, Stem Cell. 26 (2008) 1047–1055, https://doi.org/10.1634/stemcells.2007-0737.
[55] X. Han, Z. Liu, M.C. Jo, K. Zhang, Y. Li, Z. Zeng, N. Li, Y. Zu, L. Qin, CRISPR-Cas9 delivery to hard-to-transfect cells via membrane deformation, Sci. Adv. 1 (2015), e1500454, https://doi.org/10.1126/sciadv.1500454.
[56] M.E. Kizer, Y. Deng, G. Kang, P.E. Mikael, X. Wang, A.J. Chung, Hydroporator: a hydrodynamic cell membrane perforator for high-throughput vector-free nanomaterial intracellular delivery and DNA origami biostability evaluation, Lab Chip 19 (2019) 1747–1754, https://doi.org/10.1039/C9LC00041K.
[57] P. Chakrabarty, P. Gupta, K. Illath, S. Kar, M. Nagai, F.G. Tseng, T.S. Santra, Microfluidic mechanoporation for cellular delivery and analysis, Mater, Today Bio 13 (2022), 100193, https://doi.org/10.1016/j.mtbio.2021.100193.
[58] M.G. Booty, K.A. Hlavaty, A. Stockmann, E.I. Ozay, C. Smith, L. Tian, E. How, D. Subramanya, A. Venkitaraman, C. Yee, O. Pryor, K. Volk, K. Blagovic, I. Vicente-Suarez, D. Yarar, M. Myint, A. Merino, J. Chow, T. Abdeljawad, H. An, S. Liu, S. Mao, M. Heimann, L. Talarico, M.K. Jacques, E. Chong, L. Pomerance, J.T. Gonzalez, U.H. von Andrian, K.F. Jensen, R. Langer, H. Knoetgen, C. Trumpfheller, P. Umaña, H. Bernstein, A. Sharei, S.M. Loughhead, Microfluidic squeezing enables MHC class I antigen presentation by diverse immune cells to elicit CD8$^+$ T cell responses with antitumor activity, J. Immunol. 208 (2022) 929–940, https://doi.org/10.4049/jimmunol.2100656.
[59] A.M. Vargason, A.C. Anselmo, S. Mitragotri, The evolution of commercial drug delivery technologies, Nat. Biomed. Eng. 5 (2021) 951–967, https://doi.org/10.1038/s41551-021-00698-w.

[60] L. Debbi, S. Guo, D. Safina, S. Levenberg, Boosting extracellular vesicle secretion, Biotechnol. Adv. 59 (2022), 107983, https://doi.org/10.1016/j.biotechadv.2022.107983.
[61] A. Grangier, J. Branchu, J. Volatron, M. Piffoux, F. Gazeau, C. Wilhelm, A.K.A. Silva, Technological advances towards extracellular vesicles mass production, Adv. Drug Deliv. Rev. 176 (2021), 113843, https://doi.org/10.1016/j.addr.2021.113843.
[62] X. Ding, M.P. Stewart, A. Sharei, J.C. Weaver, R.S. Langer, K.F. Jensen, High-throughput nuclear delivery and rapid expression of DNA via mechanical and electrical cell-membrane disruption, Nat. Biomed. Eng. 1 (2017) 39, https://doi.org/10.1038/s41551-017-0039.
[63] Z. Li, X. Zhou, M. Wei, X. Gao, L. Zhao, R. Shi, W. Sun, Y. Duan, G. Yang, L. Yuan, In vitro and in vivo RNA inhibition by CD9-HuR functionalized exosomes encapsulated with miRNA or CRISPR/dCas9, Nano Lett. 19 (2019) 19–28, https://doi.org/10.1021/acs.nanolett.8b02689.